Neurobiology of Disease 148 (2021) 105162

Contents lists available at ScienceDirect

Neurobiology of Disease

journal homepage: www.elsevier.com/locate/ynbdi

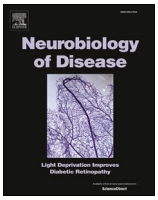

PPAR gamma agonist leriglitazone improves frataxin-loss impairments in cellular and animal models of Friedreich Ataxia

Laura Rodríguez-Pascau [a], Elena Britti [b,1], Pablo Calap-Quintana [c,d,1], Yi Na Dong [e], Cristina Vergara [f], Fabien Delaspre [b], Marta Medina-Carbonero [b], Jordi Tamarit [b], Federico V. Pallardó [c,d], Pilar Gonzalez-Cabo [c,d], Joaquim Ros [b], David R. Lynch [e], Marc Martinell [a,f], Pilar Pizcueta [a,*]

[a] Minoryx Therapeutics SL., Mataró 08302, Barcelona, Spain
[b] Departament de Ciències Mèdiques Bàsiques, IRBLleida. Universitat de Lleida, Lleida 25198, Spain
[c] Department of Physiology, Faculty of Medicine and Dentistry, University of Valencia-INCLIVA, Valencia 46010, Spain
[d] CIBER de Enfermedades Raras (CIBERER), Valencia, Spain
[e] Department of Pediatrics and Neurology, The Children's Hospital of Philadelphia, Philadelphia, PA 19104, USA
[f] Minoryx Therapeutics BE., Gosselies 6041, Charleroi, Belgium

ARTICLE INFO

Keywords:
Friedreich Ataxia
Frataxin
Neurodegeneration
Mitochondrial function
Dorsal root ganglia neurons
Cardiomyocytes
FRDA fibroblasts
YG8sR
Leriglitazone
PPARγ agonist

ABSTRACT

Friedreich ataxia (FRDA), the most common autosomal recessive ataxia, is characterized by degeneration of the large sensory neurons and spinocerebellar tracts, cardiomyopathy, and increased incidence in diabetes. The underlying pathophysiological mechanism of FRDA, driven by a significantly decreased expression of frataxin (FXN), involves increased oxidative stress, reduced activity of enzymes containing iron-sulfur clusters (ISC), defective energy production, calcium dyshomeostasis, and impaired mitochondrial biogenesis, leading to mitochondrial dysfunction. The peroxisome proliferator-activated receptor gamma (PPARγ) is a ligand-activated transcriptional factor playing a key role in mitochondrial function and biogenesis, fatty acid storage, energy metabolism, and antioxidant defence. It has been previously shown that the PPARγ/PPARγ coactivator 1 alpha (PGC-1α) pathway is dysregulated when there is frataxin deficiency, thus contributing to FRDA pathogenesis and supporting the PPARγ pathway as a potential therapeutic target. Here we assess whether MIN-102 (INN: leriglitazone), a novel brain penetrant and orally bioavailable PPARγ agonist with an improved profile for central nervous system (CNS) diseases, rescues phenotypic features in cellular and animal models of FRDA. In frataxin-deficient dorsal root ganglia (DRG) neurons, leriglitazone increased frataxin protein levels, reduced neurite degeneration and α-fodrin cleavage mediated by calpain and caspase 3, and increased survival. Leriglitazone also restored mitochondrial membrane potential and partially reversed decreased levels of mitochondrial Na^{+}/Ca^{2+} exchanger (NCLX), resulting in an improvement of mitochondrial functions and calcium homeostasis. In frataxin-deficient primary neonatal cardiomyocytes, leriglitazone prevented lipid droplet accumulation without increases in frataxin levels. Furthermore, leriglitazone improved motor function deficit in YG8sR mice, a FRDA mouse model. In agreement with the role of PPARγ in mitochondrial biogenesis, leriglitazone significantly increased markers of mitochondrial biogenesis in FRDA patient cells. Overall, these results suggest that targeting the PPARγ pathway by leriglitazone may provide an efficacious therapy for FRDA increasing the mitochondrial function and biogenesis that could increase frataxin levels in compromised frataxin-deficient DRG neurons. Alternately, leriglitazone improved the energy metabolism by increasing the fatty acid β-oxidation in frataxin-deficient cardiomyocytes without elevation of frataxin levels. This could be linked to a lack of significant mitochondrial biogenesis and cardiac hypertrophy.

Abbreviations: FRDA, Friedreich Ataxia; FXN, frataxin; PPARγ, peroxisome proliferator-activated receptor gamma; PGC-1α, PPARγ coactivator 1 alpha; CNS, central nervous system; DRG, dorsal root ganglia; NCLX, mitochondrial Na^{+}/Ca^{2+} exchanger; ISC, iron-sulfur clusters; KIKO, knock in-knock out mouse model of FRDA; NRVMs, neonatal rat ventricular myocytes; FFA, Free Fatty Acids; CPT-1, carnitine palmitoyltransferase-1; MCAD, medium-chain acyl-CoA dehydrogenase..

* Corresponding author at: Minoryx Therapeutics SL., Av. Ernest Lluch 32 - TCM3, 08302 Mataró, Barcelona, Spain.
E-mail address: ppizcueta@minoryx.com (P. Pizcueta).

[1] These authors contributed equally to the work.

https://doi.org/10.1016/j.nbd.2020.105162
Received 6 August 2020; Received in revised form 14 October 2020; Accepted 3 November 2020
Available online 7 November 2020

The results reinforced the different tissue requirement in FRDA and the pleiotropic effects of leriglitazone that could be a promising therapy for FRDA.

1. Introduction

Friedreich ataxia (FRDA; OMIM #229300) is an autosomal recessive neurodegenerative disease characterized by progressive gait and limb ataxia, sensory loss, weakness, dysarthria, and hypertrophic cardiomyopathy. It is caused by mutations in the frataxin gene (*FXN*), most commonly expanded GAA triplet repeats in its first intron resulting in transcriptional silencing and consequent reduction in the expression of the protein frataxin (Campuzano et al., 1996). Frataxin is an ubiquitously expressed mitochondrial protein involved in iron homeostasis, biosynthesis of iron-sulfur clusters (ISC), and energy production in the cell (Bencze et al., 2006; Bulteau et al., 2004; Gerber et al., 2003; Stehling et al., 2004; Vaubel and Isaya, 2013; Wilson and Roof, 1997). Reduction in frataxin expression leads to decreased activity of ISC containing enzymes such as aconitase and the mitochondrial respiratory chain complexes (Bradley et al., 2000), calcium dyshomeostasis (Abeti et al., 2018; Bolinches-Amorós et al., 2014; Mincheva-Tasheva et al., 2014; Mollá et al., 2019), mitochondrial iron accumulation, oxidative stress, and consequently cell death, with the primary affected sites being large sensory neurons of the dorsal root ganglia (DRG), the dentate nucleus of the cerebellum, and a variety of other central nervous system (CNS) cells (Campuzano et al., 1997; Koeppen, 2011; Koeppen et al., 2009, 2007). However, cardiomyopathy is the most prominent cause of death for FRDA patients (Tsou et al., 2011). Currently there is no specific therapy to prevent the progression of FRDA (Clay et al., 2019).

Peroxisome proliferator-activated receptor gamma (PPARγ) is a transcription factor that plays essential roles in regulating fundamental cellular processes such as differentiation, development and metabolism (carbohydrate and lipid); it is also a key regulator of mitochondrial function, biogenesis and anti-oxidation effects. PPARγ regulates the expression of PPARγ coactivator 1 alpha (PGC-1α), a coactivator of PPARγ and a master regulator of mitochondrial biogenesis (Puigserver et al., 1998; Puigserver and Spiegelman, 2003). Mitochondrial biogenesis deficits occur in the cerebellum of FRDA knock in-knock out mouse model (KIKO) (Lin et al., 2017), and decreased PGC-1α levels and transcriptional activity have been also observed in multiple cell types from FRDA patients and FRDA mouse models (Coppola et al., 2009; Marmolino et al., 2010). Concomitantly, decreased mitochondria copy number and mitochondrial DNA levels as well as disrupted mitochondrial networks have been observed in FRDA cells (Dong et al., 2019; Jasoliya et al., 2017), suggesting that abnormalities of mitochondrial function and biogenesis deficits can underlie the pathophysiology of FRDA. Mitochondrial damage is also observed in frataxin-deficient cardiomyocytes affecting the energetic needs of the heart, which mainly depend on oxidative catabolism of fatty acids (Obis et al., 2014; Purroy et al., 2020). Thus, upregulation of PGC-1α using PPARγ agonists may be an appealing therapeutic approach. In this line, it was shown that activation of the PGC-1α pathway with PPARγ agonist pioglitazone reversed PGC-1α down-regulation in primary fibroblasts from FRDA patients suggesting PPARγ agonists as a potential therapeutic approach for FRDA (Marmolino et al., 2010).

Leriglitazone (5-[[4-[2-[5-(1-hydroxyethyl)pyridin-2-yl]ethoxy] phenyl]methyl]-1,3-thiazolidine-2,4-dione hydrochloride) is the hydrochloride salt of the active metabolite M4 (M-IV) of pioglitazone (Actos®, Takeda). Leriglitazone is a novel and orally bioavailable PPARγ agonist that engages the target receptor at the levels required for efficacy within the CNS. Compared with other PPARγ agonists, leriglitazone shall be used to treat CNS diseases thanks to its adequate brain penetration, good bioavailability, and safety profile (Poli et al., 2020). In the present study, we examined the effect of leriglitazone on neurons, cardiomyocytes, and fibroblasts cell models, and on behavioural phenotypes in vivo in the YG8sR mouse model of FRDA.

2. Materials and methods

2.1. Human skin fibroblasts culture

Human skin fibroblasts primary cultures derived from control and FRDA patient were obtained from skin biopsy. Fibroblast cell lines F281 (753/808 GAA repeats), 4654 (333/733 GAA repeats) and 4675 (600/1200 GAA repeats) were obtained from the bank of FRDA patient fibroblasts established by Dr. Marek Napierala (The University of Alabama at Birmingham, Birmingham, AL) and Dr. David R. Lynch (The Children's Hospital of Philadelphia, Philadelphia, PA). Fibroblasts were cultured in 5% CO_2 humidified atmosphere in Dulbecco's Modified Eagle Medium (DMEM): Nutrient Mixture F-12 containing 1% penicillin/streptomycin, 1% non-essential amino acid and 10% fetal bovine serum. Cells were treated with leriglitazone at increasing concentrations up to 600 nM for two days and then collected in Laemmli sample buffer (50 mM Tris-HCl, pH 6.8, 2% SDS, 5 mM EDTA, 0.1% bromophenol blue, 10% glycerol, and 2% β-mercaptoethanol) followed by Western blot analysis.

2.2. Isolation and culture of primary rat DRG sensory neurons

DRGs were extracted from neonatal Sprague–Dawley rats (P3–P4) and dissociated with 0.05% trypsin (Sigma-Aldrich, St. Louis, MO). Ganglia were mechanically disrupted with a pipette tip until obtaining a single cell suspension in culture medium supplemented with DNAse I grade II at a final concentration of 3 mg/ml (Roche Diagnostics, Basel, Switzerland), which was centrifuged at 800 rpm through 7.5% BSA solution (Sigma-Aldrich, St. Louis, MO) for 5 min, followed by resuspension in enriched neurobasal culture medium consisting of 2% horse serum, 2% B27 supplement, 0.5 mM L-glutamine, 100 U/ml penicillin plus 100 ng/ml streptomycin (All from Thermo Fisher Scientific, Waltham, MA) and supplemented with murine β-nerve growth factor at 50 ng/ml (PeproTech, Rocky Hill, NJ). To prevent the growth of non-neuronal cells, culture medium was supplemented with the anti-mitotic agent Aphidicolin at 3.4 μg/ml (Sigma-Aldrich, St. Louis, MO). After 1 h of pre-plating in p60 tissue dish (Corning Inc., Corning, NY) at 37 °C/5%CO_2, the cells were then plated in a 24-well tissue dish (Corning Inc., Corning, NY) pre-treated with 0.1 mg/ml of collagen (Sigma-Aldrich, St. Louis, MO) at a density of 10,000–20,000 cells/well. After 1–2 days, lentiviral transduction was performed and 6 h later the medium containing lentivirus was replaced by fresh culture medium containing leriglitazone at different concentrations (50 nM, 100 nM, 300 nM, 500 nM) or equal amount of vehicle (DMSO) for five days. The culture medium, containing leriglitazone, was changed at 72 h.

2.3. Isolation and culture of rat ventricular myocytes

Neonatal rat ventricular myocytes (NRVMs) were obtained as described previously (Obis et al., 2014) with some modifications. Briefly, ventricles from newborn Sprague–Dawley rats (P3-P4) were minced and cells were isolated by 3 subsequent digestions at 37 °C with 150 U/ml of type-2 collagenase (Worthington, Lakewood, NJ). Non-cardiomyocyte cells were separated by differential pre-plating. Cardiomyocytes were seeded on 0.2% gelatin-coated culture dishes at $7.5–10^4$ cells/cm^2 and cultured in medium consisting of DMEM: M199 (3:1), 5 mM glucose, 8% horse serum, 4% foetal bovine serum, glutaMAX and HEPES (all from GIBCO, Waltham, MA). To inhibit the proliferation of cardiac fibroblasts, cells were treated with 10 μg/ml

mitomycin C (Sigma-Aldrich, St. Louis, MO) for 4 h after seeding. Cardiomyocyte purity was checked by immunofluorescence with a specific cardiac α-actinin antibody (Sigma-Aldrich, St. Louis, MO). Fatty acid-albumin solutions were used for Free Fatty Acids (FFA) supplementation of the culture medium. A commercial oleic and linoleic-albumin solution was used to provide these unsaturated fatty acids. Saturated fatty acid-albumin solutions where prepared as described previously (Obis et al., 2014; Purroy et al., 2018). These solutions of FFA were added to the medium with a final concentration of 30 μM oleic, linoleic and stearic acid, and 60 μM of palmitic. Lentiviral transduction was performed 4 h after plating and 20 h later the medium containing lentivirus was substituted by fresh culture medium containing leriglitazone at different concentrations (0.5 μM, 2 μM) and kept for seven days. The culture medium, containing leriglitazone was changed every 24 h.

2.4. Lentivirus titration and transduction

Lentiviral particles were produced as described (Britti et al., 2018; Purroy et al., 2018). Briefly, the shRNA lentiviral plasmids (pLKO.1-puro) for human/mouse/rat frataxin were purchased from Sigma. The RefSeq used was NM-008044, which corresponds to mouse frataxin. The Clone used was TRCN0000197534, here referred as FXN1. The vector SHC002, a non-targeted scrambled sequence, served as a control (Scr). Lentivirus were tittered using the Quicktitter Lentivirus ELISA kit (Cell Biolabs, Catalogue #: VPK-108-H) which detects the levels of p24 protein. For transduction of NRVMs, 5.5 ng p24/1000 cells were added to the medium 4 h after plating, and 20 h later, the culture medium was replaced with fresh medium. Cells were maintained up to seven days in culture (Purroy et al., 2018). For lentiviral transduction of DRG neurons, cells were plated in 24-well dishes, and medium containing lentivirus particles (20 ng p24/1.000 cell) was added 24 h later. This protocol provided transduction efficiency greater than 70%, according to the GFP control vector. DRG neurons were used after five days in culture (Britti et al., 2018).

2.5. Immunofluorescence staining

Five days after lentiviral transduction and leriglitazone treatment, frataxin depleted DRG neurons seeded on collagen treated coverslips (10,000 cells/per coverslip) were washed twice with PBS and fixed in 4% paraformaldehyde at room temperature (RT) for 20 min. Cells were then washed with PBS, permeabilized with 0.5% TritonX100 at RT for 30 min and blocked with 1% BSA/ 0.2% Triton X100 in PBS at RT for 2 h. An antibody to β-III Tubulin (at 1/250 dilution) was then added and incubated overnight at 4 °C. After washing with PBS, cells were incubated with Alexa Fluor 488 secondary antibody (Invitrogen, Carlsbad, CA at 1/250) in the dark for one hour at 37 °C followed by nuclei staining with DAPI for 5 min. Coverslips were then mounted with Mowiol mounting medium (Sigma-Aldrich, St. louis, MO). Immunofluorescent images were taken with an Olympus BX51 microscope with a x20 lens and an Olympus U-MNUA2 filter for Dapi and Olympus U-MNBA3 filter for β-III Tubulin.

2.6. Survival and neurite degeneration analysis of DRG neurons

Neuronal survival was measured with a × 16 lens and cross-marked wells. Neurons at zero and 5 days were counted at four fields per cross-marked well, using three wells per condition tested. Neurite degeneration was measured with a x20 lens (plus zoom x1.6) and a grid, which was created over each image with NIH Image J with the grid plugin (Image size 680 × 512 and line area 10,000 pixels). Healthy and degenerated neurites (displaying neurofilament aggregates) were counted at three grid fields per image and at least three images per well were analysed. For each condition, three different wells were used. Experiments were repeated at least three times.

2.7. Assessment of mitochondrial membrane potential (ΔΨm) with JC-1

The ΔΨm was assessed using the dual-emission, mitochondrion-specific, lipophilic, cationic dye 5,5′,6,6′-tetrachloro-1,1′,3,3′-tetraethylbenzimidazoly-carbocyanine iodide (JC-1) (Abcam, Cambridge, MA, Catalogue #: Ab141387) diluted in DMSO, to identify depolarized (green) or polarized (red) mitochondria. Cultures of DRG neurons were plated in a twenty-four-well tissue dish and analysed for JC-1 at 72 h after lentivirus transduction. The cells were first incubated at 37 °C 5% CO_2 with 5 μg/ml JC-1 in neurobasal medium for 30–35 min and then washed with PBS at 37 °C. Images were taken using an Olympus FluoView IX71 microscope with objective 10× + 1.6× capable of detecting the J-aggregate form of JC-1 using an excitation of 460–500 nm and an emission of 510–550 nm (filter Omega XF116-2), the monomeric form of JC-1 at an excitation of 520–550 nm and an emission higher than 510 nm (filter Olympus U-MWIB2), and both forms at an excitation of 460–490 nm and an emission higher than 510 nm (filter Olympus U-MWIG2). Fluorescence is green/yellow in mitochondria with low ΔΨm (monomers) and red/orange in those with high ΔΨm (aggregates). Pictures were analysed with the Image J software. The region of interest (ROI) was the entire image itself using the filter for both forms of JC-1 and the filter for aggregates, each image was split into three 8-bit grayscale images containing the red and green components of the original. Once we considered that the split image taken with the filter for aggregates also contained the green component, we corrected the fluorescence intensity using this formula:

Real green fluorescence intensity = Green fluorescence Intensity – (Red fluorescence intensity * factor X).
Factor X = green fluorescence intensity/red fluorescence intensity from the image with the filter for aggregates.

Depolarization is indicated by an increase in the real green/red fluorescence intensity ratio.

2.8. Subcellular lipid labelling and image analysis

For labelling lipid droplets, cells were washed with PBS and loaded with 5 μM BODIPY (493/503) (Invitrogen, Carlsbad, CA) for 20 min at 37 °C. For nuclei staining, Hoechst 33258 (0.05 μg/ml) was used. Cells were washed again with PBS and fluorescent images were captured with a x20 lens using an Olympus IX71 microscope equipped with epifluorescence optics and a DP70 CCD camera. The used values were area of lipid droplets per nuclei.

2.9. Western blot

Frataxin deficient rat DRG neuron cultures were rinsed three times in ice-cold PBS (pH 7.4) and lysed with a buffer containing 2% SDS, 125 mM Tris and protease inhibitors (Roche) to obtain crude extracts used for SDS–polyacrylamide gel electrophoresis (SDS-PAGE). Cultured human fibroblasts were collected in Laemmli sample buffer (50 mM Tris-HCl, pH 6.8, 2% SDS, 5 mM EDTA, 0.1% bromophenol blue, 10% glycerol, and 2% β-mercaptoethanol). A sample (15–50 μg) of total protein was boiled for 5 min and then loaded onto NuPAGE 4–12% Bis-Tris gel (fibroblasts) or SDS-polyacrylamide gels (DRGs). Following SDS-PAGE, proteins were transferred to nitrocellulose (Sigma-Aldrich, Catalogue #: 10600093) or PVDF membranes (Millipore, Catalogue #: IPVH00010), blocked with 3% dry milk, and incubated with antibodies against: frataxin (Abcam Catalogue #: ab219414), GRP75 (Abcam, Cambridge, MA, Catalogue #: ab2799), PGC-1α (Abcam, Cambridge, MA, Catalogue #: ab77210), NCLX (LifeSpan BioSciences, Seattle, WA, Catalogue #: LS-C102072), α-fodrin (ENZO Life Science, Farmingdale, NY, Catalogue #: BML-FG6090-0100), beta tubulin (Cell Signaling, Danvers, MA, Catalogue #: 5568) all at dilution 1/1000, frataxin (Abcam, Cambridge, MA at 1/500, Catalogue #: ab175402) and β-actin

(Chemicon-EMD Millipore, at 1/250000, Catalogue #: MABT825). Blots were then incubated with appropriate horseradish peroxidase-conjugated secondary antibodies and developed with enhanced chemiluminescence (Pierce, Rockford, IL).

2.10. Animals

The mouse model of FRDA used in this study was the *Fxn*^{tm1Mkn} Tg (*FXN*)YG8Pook/2 J (YG8sR) (Jackson Laboratory, stock number 024113) which carries the mouse frataxin knockout allele (Fxn^{-}) and a single copy integration of the human FXN YAC transgene $(GAA)_{250–300}$. As control mice, we used the C57BL/6 J, which shares the genetic background of the YG8sR mice. All mice were housed in an environment of 12 h light/dark cycle, temperature of 25 ± 2 °C, 55% humidity, and ad libitum standard diet and water. Studies on C57BL/6 J mice and YG8sR were performed in accordance with standard regulations and were approved by Bioethics subcommittee of the University of Valencia.

2.11. Motor performance assessment of YG8sR mice

We assessed motor function of the YG8sR mouse as the phenotype of interest to study the effect of the compound leriglitazone. As control mice, we used the C57BL/6 J. The mice were subjected to the rotarod test, the pole test, and the balance beam test once a month starting from month 3 up to month 11. The mice were initially trained for 4 consecutive days before the first trial until each animal performed the different tests properly. The treatment with leriglitazone was started for a proportion of the YG8sR mice after the motor tests of month four were completed and continued until the sacrifice at eleven months of age. The animals were fed ad libitum and the compound was administered as part of the food at a concentration of 0.06% (equivalent to 50 mg/kg/day). The number of animals in each group were 12 C57BL/6 J, 10 YG8sR and 11 YG8sR + leriglitazone.

In the rotarod test, an automated 4-lane accelerating RotaRod (TSE) was used to examine motor coordination. This test was performed during five consecutive days, and consisted of four trials per day, with intervals of 10 min between each trial. The first day was used only to retrain the animals. For each trial, the mice were placed on the rotating rod, which accelerates from 4 to 40 rpm over the trial time of 5 min. The measure obtained is the time the mouse is able of staying running on top the cylinder until it falls (latency time in seconds) and the score considered for each month is the average of all the trials.

The pole test predominantly analyses extrapyramidal motor locomotion. This test consisted of 5 consecutive trials, one day per month. The mouse was placed head upwards on the top of a pole, whose rough surface facilitates the mouse grabbing to the beam. We register the capacity of turning around and to descend the vertical pole for each mouse. A maximum time of 120 s was allowed to execute the task. The measure obtained for each month is the percentage of trials the mice were able to turn around and descend the pole.

Sensory-motor coordination was tested using the balance beam test with 26 and 12 mm wide bars. Every month, each mouse was given three trials per beam. In the test, the mice are placed at the end of the 1 m long bars elevated 50 cm above the floor. We measured the time required by the mice to cross the bars, and for each month we take as score the average of the best two trials for each bar (latency time in seconds).

2.12. UPLC-MS/MS analysis

Levels of leriglitazone were quantified in plasma samples from YG8sR mice after two weeks of administration by UPLC-MS/MS. Linearity was established by a calibration curve with 8 levels different from 0 prepared by spiking matrix with known concentrations of analytes. A known concentration of internal standard was added in each sample. Acceptance criteria: the deviation of standards used to perform the calibration curve should be ≤15% from nominal concentration, except in the LOQ, which can be 20%.

2.13. Statistical analysis

GraphPad. PRISM® software (GraphPad Software Inc.) was used to generate the graphs and to perform statistical analysis. The results are expressed as mean ± SEM. Statistical test performed was stated in the corresponding figure legend. Significant *p*-values: $^{*}p < 0.05$; $^{**}p < 0.01$; $^{***}p < 0.001$; $^{****}p < 0.0001$ were considered.

3. Results

3.1. Leriglitazone increases frataxin amounts in frataxin-deficient DRG neurons

To investigate whether leriglitazone has a positive impact on frataxin levels, we first treated frataxin-deficient rat primary DRG neuron cultures. For this purpose, DRG neurons were transduced with lentivirus carrying FXN shRNA (FXN1) to reduce the endogenous expression level of frataxin, or scrambled shRNA (Scr) as control condition for frataxin endogenous levels. Crude extracts obtained after five days of leriglitazone treatment were analysed by western blotting and the results are shown in Fig. 1. As previously reported (Britti et al., 2018), lentivirus transduction with FXN1 decreased frataxin levels in DRG neurons by 58% compared with lentivirus containing Scr (Fig. 1) (58% decrease from Scr vehicle, $p < 0.0001$, $n = 8$). Treatment of frataxin-deficient DRG neurons with leriglitazone at 500 nM exerted a significant 48% increase of frataxin

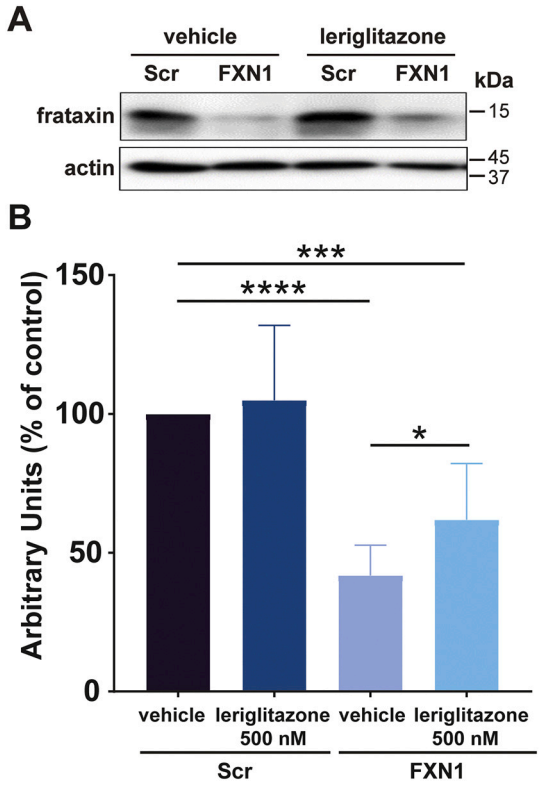

Fig. 1. Leriglitazone increases frataxin levels in frataxin-deficient DRG neurons. (A) Crude extracts of primary cultures of frataxin-deficient DRG neurons (FXN1) and controls (Scr), obtained as described in materials and methods, were tested for frataxin amounts after leriglitazone treatment at 500 nM by Western blot. Actin was used as a loading control. (B) Quantitative analysis of frataxin levels expressed as % of control (Scr vehicle). Data is expressed as mean ± SEM from 8 independent experiments and was analysed by Student's *t*-test ($^{*}p < 0.05$, $^{**}p < 0.01$, $^{***}p < 0.001$, $^{****}p < 0.0001$).

compared to vehicle treated cells (Fig. 1).

3.2. Leriglitazone rescues cell survival, neurite degeneration and mitochondrial function in frataxin-deficient DRG neurons

Frataxin depletion in DRG neurons promotes neurite degeneration indicated by the formation of neurofilament aggregates and leads to depolarization of mitochondria, calcium dysregulation and apoptotic cell death (Mincheva-Tasheva et al., 2014). Thus, we examined whether leriglitazone rescues the neuronal phenotype and cell viability in frataxin-deficient DRG neurons. Briefly, DRG neurons were transduced with lentivirus carrying FXN1 or Scr and treated with leriglitazone for 5 days followed by survival, neurite degeneration, mitochondrial membrane potential, and western blot analysis, as detailed in material and methods. Consistent with previous reports (Britti et al., 2018; Mincheva-Tasheva et al., 2014), transduction with lentivirus carrying FXN1 decreased the number of surviving DRG neurons (Fig. 2A) (48% decrease compared to Scr vehicle, $p < 0.0001$, $n = 4$). Treatment with leriglitazone increased survival of frataxin-deficient DRG neurons in a dose-dependent manner, with maximal effect at 500 nM (Fig. 2A) (44% increase over FXN1 vehicle, $p < 0.0001$, n = 4). Frataxin depletion also promoted neurite degeneration in DRG neurons as evidenced by swelling and increased neurofilament aggregates (Fig. 2B and C) (92% increase from Scr vehicle, $p < 0.0001$, $n = 3$). The treatment with leriglitazone at 500 nM decreased the number of neurofilament aggregates (Fig. 2B and C) (44% decrease from FXN1 vehicle, $p < 0.0001$, n = 3) and restored the morphology of neurites. These results indicate that leriglitazone ameliorates neurite degeneration and promotes cell survival in frataxin-deficient DRG neurons.

We next examined whether leriglitazone blocks the apoptotic events leading to α-fodrin cleavage and decreased mitochondrial membrane potential. An intracellular increase of calcium activates calcium-dependent proteases leading to the cleavage of the cytoskeletal protein, α-fodrin. Transduction of DRG neurons with lentivirus carrying FXN1 led to α-fodrin cleavage, into a non-specific 150 kDa fragment and a calpain-specific 145 kDa fragment or a caspase 3-specific 120 kDa product (Fig. 3A and B), as previously described (Purroy et al., 2018). Leriglitazone treatment (500 nM) decreased the levels of 150/145 kDa and 120 kDa fragments (Fig. 3A and B) (150/145 kDa, $p < 0.05$; 120 kDa, $p < 0.001$, $n = 8$). Similarly, DRG neurons lentiviral transduction with FXN1 increased the ratio of green/red fluorescence of JC-1 (Fig. 3C and D), indicating a decreased mitochondrial membrane potential and compromised mitochondrial function. In contrast, leriglitazone treatment restored the membrane potential close to control Scr vehicle values (Fig. 3C and D) ($p < 0.01$, n = 3). Finally, we examined whether leriglitazone affects mitochondrial Na^+/Ca^{2+} exchanger (NCLX) levels. NCLX is associated with frataxin deficiency in frataxin-deficient DRG neurons, frataxin-deficient cardiomyocytes, and lymphoblastoid cell lines from patients (Purroy et al., 2018). NCLX levels have been previously shown to decrease in frataxin deficiency which are restored either by using frataxin replacement or by the calcium

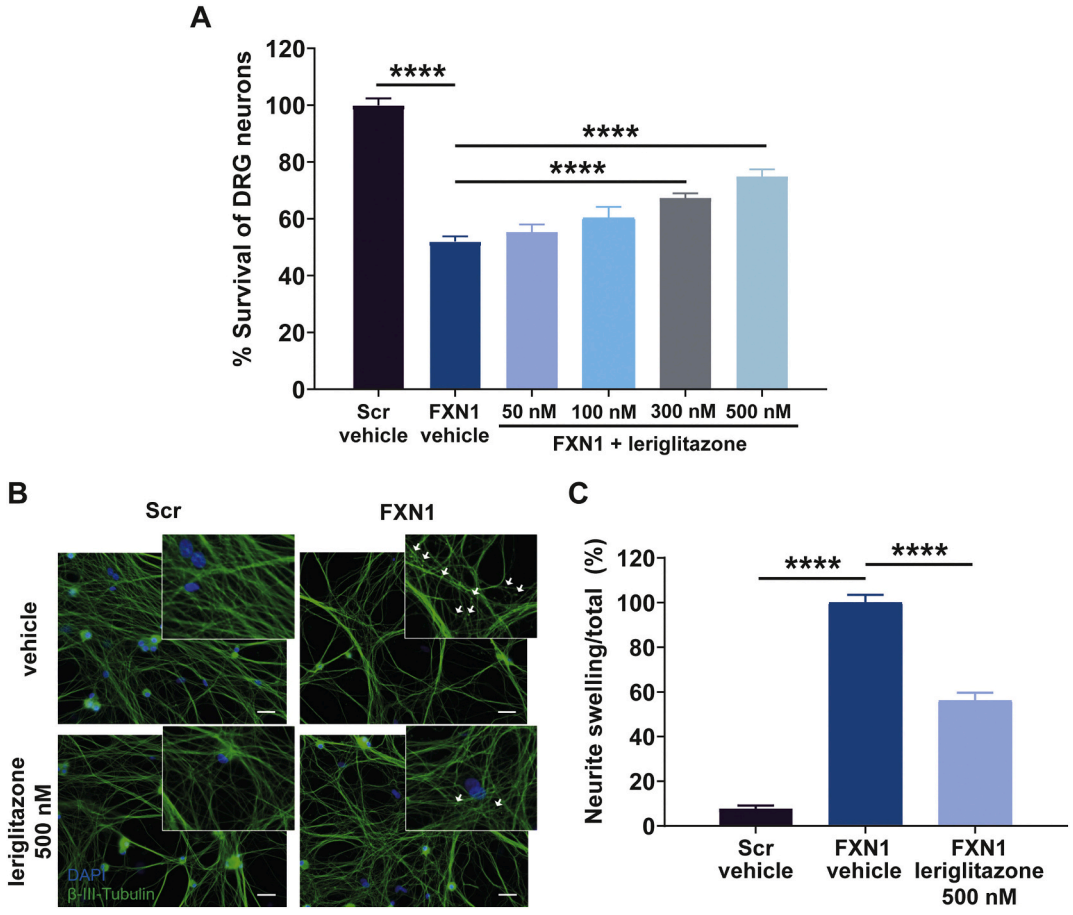

Fig. 2. Leriglitazone rescues cell survival and neurite degeneration in frataxin-deficient DRG neurons. Rat primary DRG neurons were transduced with lentivirus carrying FXN1 or Scr and treated with leriglitazone for 5 days followed by survival and neurodegeneration analysis. (A) Percentage of survival of frataxin-deficient DRG neurons in the presence of increasing concentrations of leriglitazone up to 500 nM compared to Scr vehicle. (B) Representative β-III-Tubulin immunofluorescence microscopy images of 5-day cultures treated with leriglitazone (500 nM) or vehicle solution. Arrows show neurite aggregates present only in degenerated neurons. Scale bar 30 μm. (C) Quantification of neurites aggregates versus total neurites of DRG neurons after treatment with leriglitazone (500 nM). All data is expressed as mean ± SEM and was statistically analysed by one-way ANOVA. (*$p < 0.05$, **$p < 0.01$, ***$p < 0.001$, ****$p < 0.0001$).

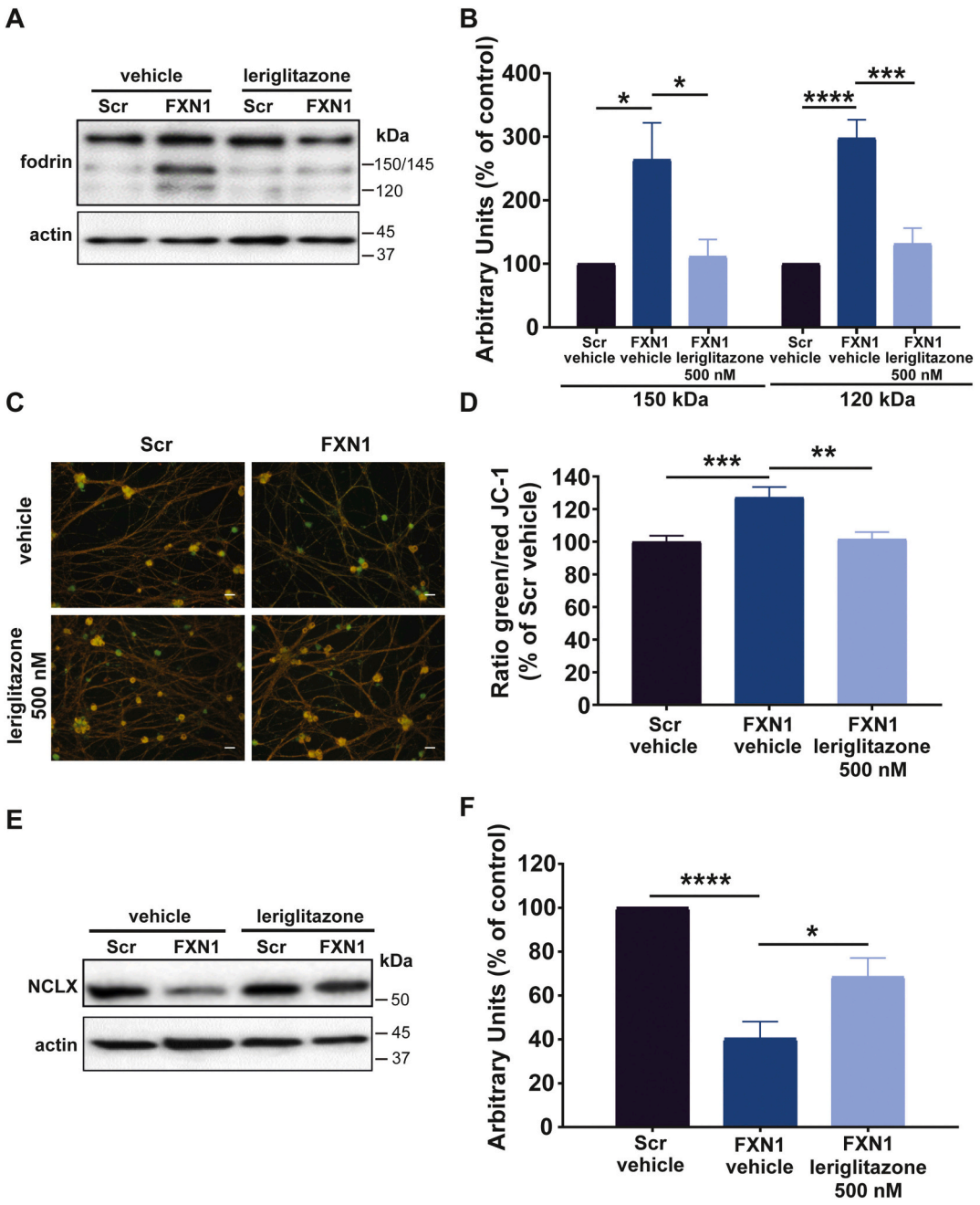

Fig. 3. Leriglitazone improves mitochondrial function in frataxin-deficient DRG neurons. Rat primary DRG neurons were transduced with lentivirus carrying FXN1 or Scr and treated with leriglitazone at 500 nM for 5 days followed by western blot or immunofluorescence analysis. (A) Representative western blot and (B) quantification of relative amounts of fragmented α-fodrin (145/150 KDa and 120 KDa) in the absence or presence of leriglitazone (500 nM) compared to Scr vehicle. (C) Representative microscopy images of DRG neurons transduced with FXN1 or Scr in the absence or presence of leriglitazone (500 nM) followed by JC-1 assay. Scale bar 30 μm. (D) Ratio green/red JC-1 assay expressed as % of Scr vehicle in the absence or presence of leriglitazone (500 nM). (E) Representative western blot and (F) quantification of relative amounts of NCLX in the absence or presence of leriglitazone (500 nM) compared to Scr vehicle. All the results are shown as mean ± SEM, and t-test and one-way ANOVA were used for the statistical analysis (*$p < 0.05$, **$p < 0.01$, ***$p < 0.001$, ****$p < 0.0001$). (For interpretation of the references to colour in this figure legend, the reader is referred to the web version of this article.)

chelator BAPTA (Purroy et al., 2018). In addition, calpains inhibition improves the NCLX levels (Britti et al., 2020). Transduction of DRG neurons with lentivirus carrying FXN1 significantly decreased the levels of NCLX in frataxin-deficient DRG neurons (Fig. 3E and F) (60% decrease from control, $p < 0.0001$, $n = 7$). Treatment with leriglitazone (500 nM) partially restored levels of NCLX (Fig. 3E and F) (69.8% increase compared to FXN1 vehicle, $p < 0.05$, n = 7). Taken together, these results would indicate that leriglitazone acts at multiple levels to slow down DRG neurons degeneration caused by frataxin deficiency, by improving mitochondrial function and calcium homeostasis.

3.3. *Leriglitazone reduces lipid droplet formation in frataxin-deficient cardiomyocytes without changing frataxin levels*

We next investigated whether leriglitazone modifies frataxin protein levels and reduces lipid droplet formation, a marker of lipid metabolism dysfunction, in frataxin-deficient cardiomyocytes. Neonatal rat

ventricular myocytes (NRVMs) were cultured and transduced with lentivirus carrying FXN1 sequence or Scr and treated with leriglitazone at two different concentrations (0.5 μM and 2 μM) for 7 days followed by western blotting to detect frataxin protein or BODIPY (493/503) staining to visualize lipid droplets. Transduction of NRVMs with lentivirus containing FXN1 led to 24% residual frataxin compared with Scr, similar to previously reported (Obis et al., 2014). Treatment with leriglitazone at 0.5 and 2 μM for 7 days did not change frataxin protein levels in frataxin-deficient cardiomyocytes (Fig. 4A and B). Thus, the effect of leriglitazone on frataxin levels was cell-type dependent since frataxin levels were increased in frataxin-deficient DRG neurons after leriglitazone treatment but no changes were observed in frataxin-deficient cardiomyocytes. Lipid droplets accumulated in frataxin deficient cardiomyocytes but not in those transduced with Scr control (Fig. 4C and D). Leriglitazone treatment (2 μM) efficiently reduced lipid droplet appearance (Fig. 4C and D) (42.3% decrease from FXN1 vehicle, $p < 0.001$, $n = 5$). No significant effect was observed at a lower concentration of leriglitazone (0.5 μM). These results indicate that leriglitazone prevents lipid accumulation in frataxin-deficient cardiomyocytes.

3.4. Leriglitazone improves motor performance in YG8sR mice

The YG8sR mouse used in the study is a *FXN* YAC transgenic mouse that is homozygous for a knockdown of the mouse frataxin gene (*Fxn*$^{-}$) and hemizygous for the YG8s transgene, which contains in a single integration site a single copy of the human *FXN* gene with a tract of ~200 GAA trinucleotide repeats. These mice are rescued from the embryonic lethality caused by the *Fxn* knockout and show a degree of glucose intolerance and insulin hypersensitivity, as well as pathological alterations in the neurons of the dorsal root ganglia (Muñoz-Lasso et al., 2020) and a mild and progressive motor deficit phenotype that resembles a FRDA-like pathology (Anjomani Virmouni et al., 2015).

We next examined whether leriglitazone rescues motor deficits in the YG8sR mice that show progressive motor dysfunction over time. C57BL/6 J mice containing the genetic background in which the YG8sR was developed were used as control. Leriglitazone was administered into the food at a concentration of 0.06% (equivalent to 50 mg/kg/day). Plasma levels of leriglitazone were quantified by UPLC-MS/MS after two weeks of administration to confirm that the drug had reached the expected levels, 15.2 ± 0.5 μg/ml, that would correspond to a concentration of 50 mg/kg/day in plasma from YG8sR mice after treatment. To determine the efficiency of leriglitazone in an animal model, a pre-clinical trial was programmed with three groups of mice: C57BL/6 J ($n = 12$), YG8sR ($n = 10$), YG8sR + leriglitazone 0.06% (equivalent to 50 mg/kg/day) ($n = 11$). Motor function was tested monthly in all mice with the rotarod, pole test and balance beam tests using the 12 and 26 mm wide beams, starting from the third month and until the time of sacrifice at month 11. Treatment with leriglitazone started from the 4th month after randomization of the YG8sR mice into two groups: YG8sR (control

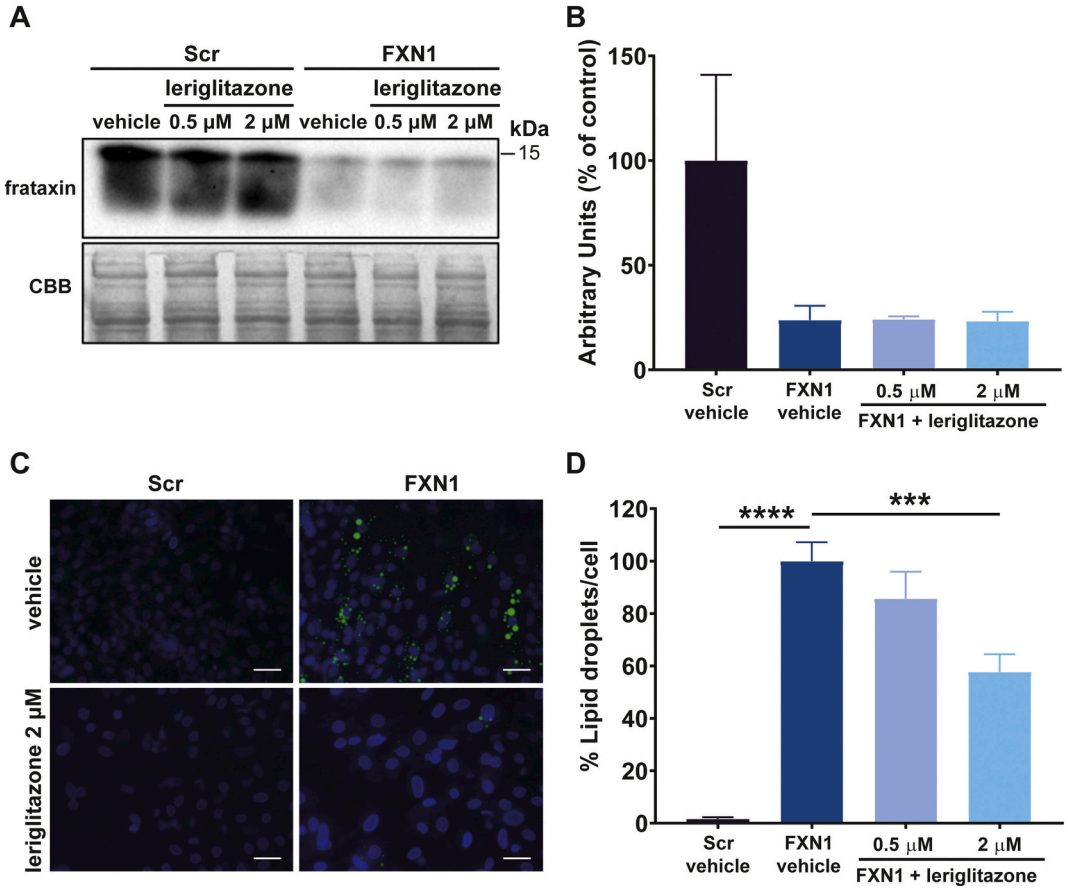

Fig. 4. Leriglitazone reduces lipid droplet accumulation in frataxin-deficient cardiomyocytes. NRVMs were transduced with lentivirus carrying frataxin shRNA (FXN1) or Scr sequence for 7 days followed by western blot for frataxin or BODIPY 493/503 staining to visualize lipid droplets. (A) Representative western blot and (B) quantification of relative amounts of frataxin in the absence and presence of leriglitazone (0.5 and 2 μM) compared to Scr vehicle. Coomassie brilliant blue (CBB) was used as a loading control. (C) Representative images of 7-day cultures treated with leriglitazone (2 μM) showing diminished lipid droplets compared with Scr vehicle control. DAPI was used for nuclei staining. Scale bar 30 μm. (D) Percentage of lipid droplets per cell after leriglitazone treatment (up to 2 μM) compared to FXN1 vehicle. Data is expressed as mean ± SEM and was statistically analysed by one-way ANOVA (*$p < 0.05$, **$p < 0.01$, ***$p < 0.001$, ****$p < 0.0001$). (For interpretation of the references to colour in this figure legend, the reader is referred to the web version of this article.)

untreated) and the YG8sR + leriglitazone. The monitoring lasted until the sacrifice at 11 months of age. Mouse body weights were recorded once a month from 3 to 11 months of age. The data obtained revealed an earlier gain of body weight in the YG8sR mice compared with C57BL/6 J, that was not reduced after treatment with leriglitazone (Supplemental Fig. S1). The execution of behavioural tests (Balance beam and rotarod) by the groups started to be differentiated at the 3rd month of age of the animals. For each test and group of mice, it is shown the performance change between the beginning of the study (average performance of months 3 and 4) and the end of the study (average performance of months 9 to 11) (Fig. 5A-D). It is also shown the progression of the performance for each month along the study (Fig. 5E-H).

On the rotarod test, YG8sR mice performed worse than the C57BL/6 J, being the differences statistically significant for months 3, 4 and 11

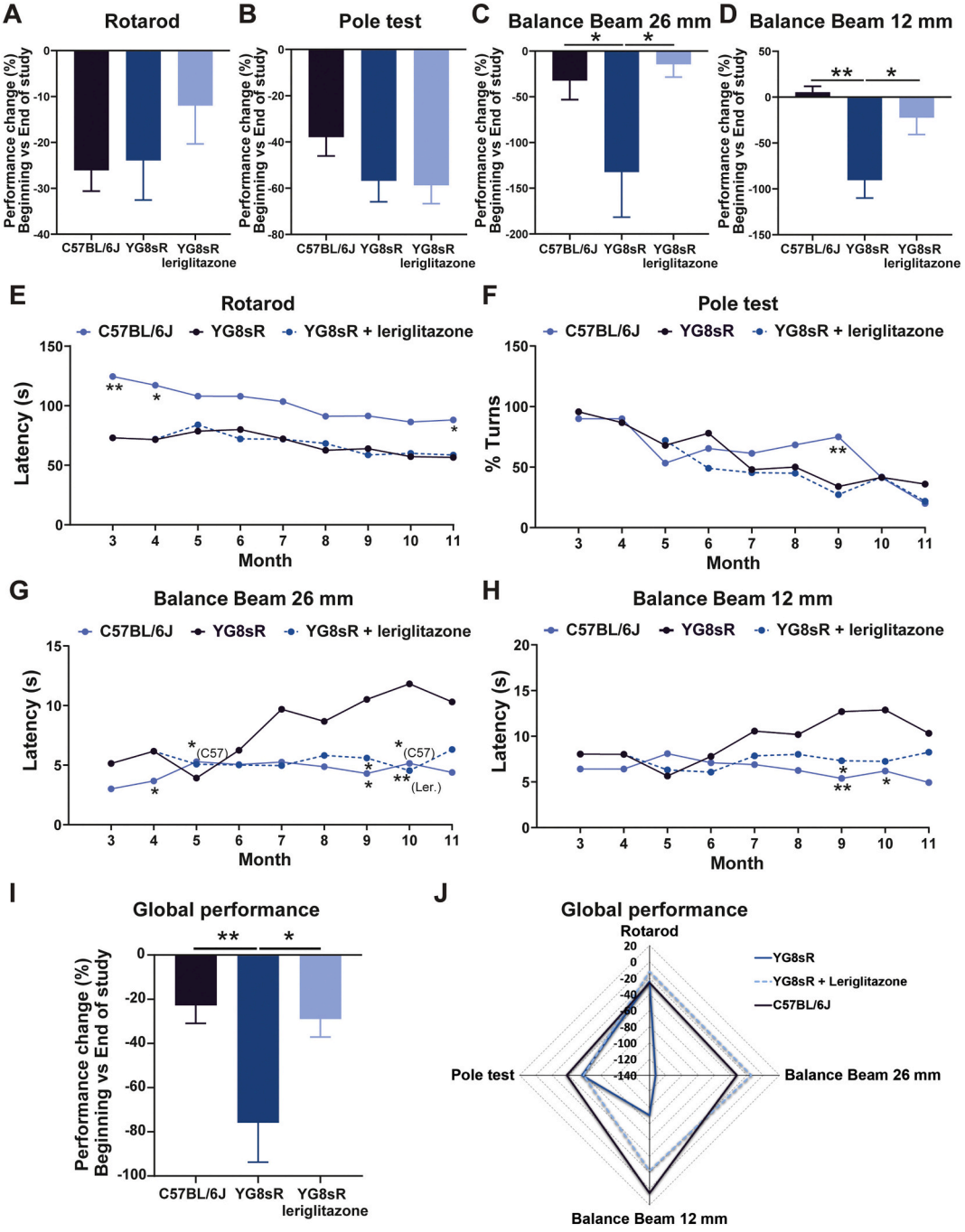

Fig. 5. Leriglitazone improves motor performance in YG8sR mouse model. (A-D) Percentage of change in performance between the beginning (average score of months 3 and 4) and the end of the study (average score of months 9 to 11) for rotarod (A), pole test (B) and balance beam test using the 26 (C) and 12 mm (D) wide bars. (*E*-H) Progression of the motor performance for all the months along the study for rotarod (E), pole test (F) and balance beam test using the 26 (G) and 12 mm (H) wide bars. The treatment with leriglitazone improve the performance of the YG8sR mice in the case of the balance beam test with the 26 mm bar (G) and 12 mm bar (H). (I) Global motor performance of the different groups calculated as the average of the performance changes in the different tests. YG8sR mice generally perform worse than the control C57BL/6 J mice can be corrected in a great extent with the treatment with leriglitazone. (J) Radial representation of the performance change of the different tests highlights that the greater differences between the groups are detected with the balance beam test. For A-D and I results are expressed as mean ± SEM and differences between groups were determined using one-way analysis of variance (ANOVA), followed by a Dunnett post hoc test. For E-H differences between groups were determined using Mixed-effects analysis, followed by a Dunnett post hoc test. Significant *p*-values: $*p < 0.05$; $**p < 0.01$.

(Fig. 5E). However, there were no differences between WT and YG8sR in the performance change percentage between beginning and end of the study due to their very similar rate of performance loss (Fig. 5A). The treatment with leriglitazone did not have a statistically significant effect on the performance of the YG8sR mice (Fig. 5A and E), despite a slight improvement in the performance change percentage (Fig. 5A).

In the pole test, the YG8sR mice performed worse than the C57BL/6 J, at least until month 10 (statistically significant difference for month 9), at which point the control mice also experimented a clear decay in their performance (Fig. 5F). In this test, the treatment did not improve the performance of the YG8sR mice either (Fig. 5B and F).

Nevertheless, in the case of the balance beam test, the treatment with leriglitazone clearly improved the performance of the YG8sR mice, both with the 26 and 12 mm wide bars. The performance of the YG8sR mice was statistically worse than C57BL/6 J for months 5, 9 and 10 in the 26 mm bar (Fig. 5G) and for months 9 and 10 in the 12 mm bar (Fig. 5H). The treatment improved the performance of the YG8sR mice, being the differences statistically significant for months 9 and 10 in the 26 mm bar (Fig. 5G) and for month 9 in the 12 mm bar (Fig. 5H). The differences in performance change between the beginning and the end of the study were also noticeable and statistically significant between the different groups (Fig. 5C-D).

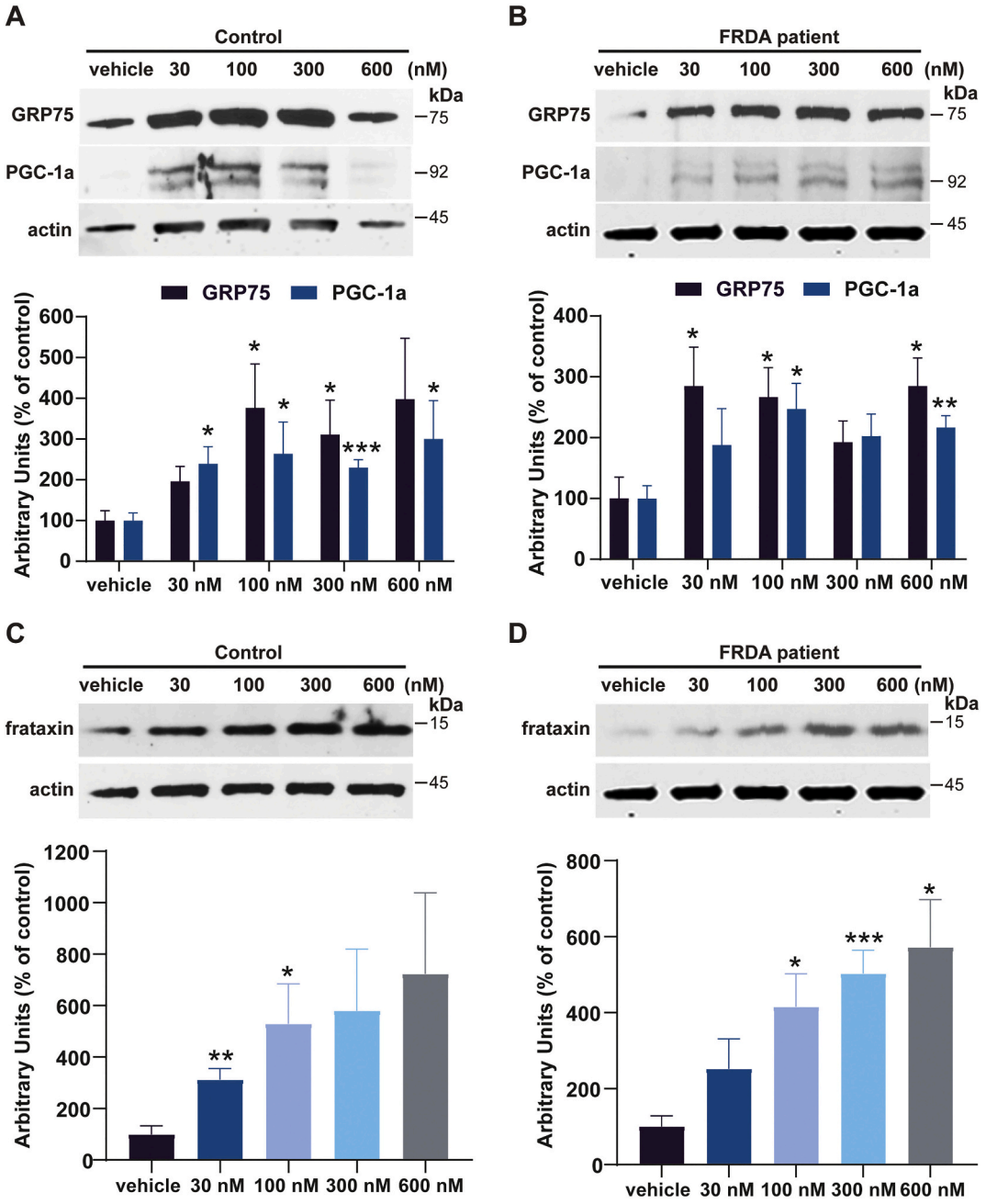

Fig. 6. Leriglitazone increases PGC-1α, GRP75 and frataxin levels in both control and FRDA patient derived-skin fibroblasts. Skin fibroblasts derived from control and FRDA patient (F281) were treated with leriglitazone for 48 h and then lysed and subjected to Western blot analysis using antibodies to PGC-1α, GRP75 and frataxin. The amount of immunoreactivity in the lysates was quantified as a percentage of vehicle. Representative blots and bar graphs demonstrate increased levels of PGC-1α and GRP75 in both control fibroblasts (A) and F281 FRDA patient fibroblasts (B) following leriglitazone treatment. Leriglitazone also increases frataxin levels in control (C) and FRDA patient-derived fibroblasts (D). Data is shown as mean ± SEM (error bars) and was analysed by Student's t-test (*$p < 0.05$, **$p < 0.01$, ***$p < 0.001$).

The YG8sR mice experienced a clear worsening in their performance in comparison with the C57BL/6 J, while the treatment with leriglitazone reversed this situation. Then, we calculated an overall global motor performance by taking the mean of the performance change percentages obtained in the rotarod, pole test and balance beam. Compared with the C57BL/6 J mice, the YG8sR demonstrated a significant impaired motor performance, and leriglitazone treatment rescued the motor function deficit of the YG8sR mice (Fig. 5I and J).

3.5. Leriglitazone increases PGC-1α, GRP75 and frataxin levels in human skin fibroblasts from control and FRDA patients

To understand the mechanism underlying the protective effect of leriglitazone on DRG neuronal survival, lipid metabolism and motor function in FRDA models, and also to investigate whether leriglitazone exhibits effect on FRDA patient cells, we examined the levels of PGC-1α in FRDA fibroblasts treated with increasing concentrations of leriglitazone for two days. Leriglitazone significantly increased PGC-1α levels in both control (Fig. 6A) and FRDA F281 patient fibroblasts (750/808 GAA repeats), (Fig. 6B). Similarly, leriglitazone significantly increased the levels of GRP75, a nuclear encoded mitochondrial chaperone downregulated in FRDA (Dong et al., 2019), in both control (Fig. 6A) and FRDA F281 patient-derived fibroblasts (Fig. 6B). These results suggest that leriglitazone promotes mitochondrial biogenesis in both control and FRDA F281 patient-derived fibroblasts. In addition, leriglitazone dose dependently increased frataxin levels in both control (Fig. 6C) and FRDA F281 patient-derived fibroblasts (Fig. 6D) with maximal effects observed at 600 nM for both control (623% increase over vehicle, 5 independent experiments, $p = 0.0575$) and patient fibroblasts (472% increase over vehicle, 4 independent experiments, $p < 0.05$). Analysis on additional FRDA patient-derived fibroblast cell lines were in the same direction (Supplemental Fig. S2). These results indicate that leriglitazone increases frataxin levels in both control and FRDA patient-derived skin fibroblasts.

4. Discussion

In the present study we have demonstrated that across several models leriglitazone rescues cellular, biochemical and behavioural features of frataxin deficiency. This includes morphological and biochemical features in cultured neurons, metabolic deficits on cardiomyocytes cultures, behavioural components in YG8sR mouse model, and biochemical aspects of cells from FRDA patients. This reversion towards a normalized phenotype is due to an improvement in the mitochondrial function and biogenesis with an increase in frataxin levels in primary DRG neurons and in patients' fibroblasts. In contrast, the optimization of lipid metabolism in frataxin-deficient cardiomyocytes is not associated with an increase in frataxin levels. Given the widely varying features of these models, these results confirm that leriglitazone represents a potential therapeutic agent.

Previous findings show that PPARγ activation by Azelaoyl-PAF increases frataxin levels in human fibroblasts (Marmolino et al., 2009). In our study with FRDA fibroblasts and in frataxin-deficient DRG neurons we observed that leriglitazone efficiently induces the expression of frataxin. Moreover, leriglitazone also induces the expression of PGC-1α and its downstream target GRP75 in both control and FRDA patient-derived fibroblasts, suggesting that the activation of PPARγ can stimulate mitochondrial biogenesis in these cells. While PGC-1α induction could increase both nuclear and mitochondrial genome encoded proteins through increased transcription, increased GRP75 could further increase the levels of these proteins through its chaperone activity, which stabilizes the frataxin precursor and increases its import and processing (Dong et al., 2019).

DRG neurons undergo apoptosis upon induction of frataxin deficiency. Leriglitazone reverses many of the apoptotic events downstream from frataxin deficiency, including fodrin cleavage and mitochondrial depolarization. While these serve as markers of apoptosis, they also in themselves play roles in the pathophysiological process. In addition, reduction of the mitochondrial calcium exchanger NCLX impairs mitochondrial calcium efflux (Purroy et al., 2018). Calcium overload can also activate mitochondrial calpains leading to further decreases of NCLX levels, by the fact that calpain inhibitors can increase its levels, thus forming a toxic positive feedback (Britti et al., 2020). Leriglitazone not only restores the levels of NCLX but also blocks calpain and caspase 3 mediated α-fodrin cleavage and recovers mitochondrial membrane potential. All these effects contribute to the protective effect of leriglitazone on DRG neurons probably by preventing the mitochondrial (intrinsic) pathway of apoptosis. On the other hand, leriglitazone could promote DRG neuronal survival through increased expression of anti-apoptotic molecules. PPARγ activation by agonists such as pioglitazone and rosiglitazone increases B-cell lymphoma 2 (Bcl-2) and B-cell lymphoma-extra large (Bcl-xL) expression and ameliorates neuronal loss in a number of cellular and animal models of neurodegenerative diseases (Fuenzalida et al., 2007; Jung et al., 2006; Qin et al., 2015; Wu et al., 2009). Thus, the expression of these anti-apoptotic proteins could protect neurons against apoptotic stimuli.

Another mechanism of action by PPARγ to take into account is the regulation of antioxidant response via PGC-1α and Nrf2. Oxidative stress is a pathogenic contributor in FRDA models (Bulteau et al., 2012; Pastore et al., 2003; Purroy et al., 2020). PGC-1α silencing by siRNA in normal fibroblasts mimics the lack of antioxidant response found in FRDA cells and stimulating PPARγ or AMPK restores the antioxidant SOD2 response in H_2O_2 stressed FRDA cells (Marmolino et al., 2010). In addition, Nrf2 expression and transcripts encoding the antioxidants, which are controlled by PGC-1α (Gureev et al., 2019), were decreased in DRG tissue in a mouse model of FRDA (Shan et al., 2013). Thus, through activation of PPARγ, leriglitazone could act at multiple levels to stimulate antioxidant response to protect DRG neurons and promote neuronal survival.

The effect of leriglitazone on frataxin-deficient cardiomyocytes emphasizes the metabolic aspects of FRDA. Lipid accumulation, as demonstrated by the formation of lipid droplets, appears in vitro in frataxin-deficient primary cultured cardiomyocytes (Obis et al., 2014), in vivo in the cardiac muscle of FRDA cardiac knockout mouse (Puccio et al., 2001), and in glia in a drosophila model of FRDA (Navarro et al., 2010). Lipid accumulation can be attributed to either increased synthesis or defective catabolism including fatty acid β-oxidation. Respiratory chain protein deficiency or pharmacologically inhibiting respiratory chain function leads to lipid accumulation (Vankoningsloo et al., 2005; Watmough et al., 1990), suggesting that mitochondrial dysfunction can be a direct cause of lipid accumulation. These alterations caused by mitochondrial impairment can have important consequences in heart cells since they need high amount of energy and mainly depend on oxidative catabolism of fatty acids for such energy. PPARγ plays critical roles in fatty acid β-oxidation through controlling the expression of its target genes. Decreasing PPARγ transcriptional activity downregulates carnitine palmitoyltransferase-1 (CPT-1), which catalyses the rate-limiting step of fatty acid β-oxidation, and medium-chain acyl-CoA dehydrogenase (MCAD) leading to lipid accumulation (Gulick et al., 1994; Vankoningsloo et al., 2005). Thus, the preventive effect of leriglitazone on lipid droplet formation in frataxin-deficient cardiomyocytes might reflect increased CPT-1 and MCAD expression by PPARγ. The protective role by PPARγ in cardiomyocytes has been recently supported by a study with PPARγ KO mice. PPARγ may prevent myocardial ischemia-reperfusion injury by modulating the Nuclear factor-κB (NF-kB)-associated inflammatory mechanisms (Lee and Kim, 2015). In addition, PPARγ gene expression is decreased in primary frataxin-deficient cardiomyocytes without changes in PGC-1α levels and with increased presence of lipid droplets compared to wild-type cardiomyocytes (Obis et al., 2014). As we show with our results, restoring PPARγ levels could alter the regulation of fatty acid β-oxidation to improve the energetic status of these cells.

The levels of the PGC-1α in the heart of FRDA patients are still controversial because a tendency of PGC-1α upregulation has been observed in a deficient frataxin cardiac cell line, which could potentially contribute to an undesired hypertrophic effect (Coppola et al., 2009). Our results showed unchanged frataxin levels in cardiomyocytes after leriglitazone treatment in contrast to the increase observed in frataxin-deficient DRG, which would indicate that mitochondrial biogenesis that could lead to a cardiac hypertrophy may not be relevant in this cell type. These results may reflect differential expression and regulation in different tissues as already suggested (Lin et al., 2017). Altogether, these data suggest that the effect of leriglitazone preventing lipid accumulation through PPARγ may be mediated preferentially by regulation of fatty acid β-oxidation and in less amount to an improvement of mitochondrial functionality.

To investigate the effect of oral leriglitazone administration on locomotor behaviour in YG8sR mouse model we used four behavioural tests that are employed to analyse cerebellar function in mice. After seven months of chronic treatment, results show that leriglitazone partly improves motor function. The performance in the rotarod and pole tests was very similar between the group of YG8sR and YG8sR + leriglitazone mice, but nevertheless an improvement was observed in the balance beam test. A global analysis of the performance of the mice showed that the YG8sR mice experiment up to 50% more decline than the control that recovered after treatment with leriglitazone.

In summary, leriglitazone protects the DRG neurons from apoptotic cell death, and improves motor function deficit in FRDA mouse model. These effects could be mediated in part by increased mitochondrial biogenesis and functionality that lead to an increase in frataxin levels. In addition, leriglitazone can reduce lipid accumulation in frataxin-deficient cardiomyocytes by improving the fatty acid β-oxidation compromised in FRDA without elevation of frataxin levels and probably linked to a lack of significant mitochondrial biogenesis and cardiac hypertrophy. The results reinforced the different tissue requirement in FRDA and the pleiotropic effects of leriglitazone that could cover the multiple features of the disease. Since leriglitazone can be administered orally with high brain penetration efficiency (Poli et al., 2020), our results support a further study of this compound in clinical settings of FRDA. Leriglitazone is currently being evaluated in a phase II clinical trial in patients with FRDA.

Declaration of Competing Interest

LRP, CV, MM and PP are current employees at Minoryx Therapeutics. MM and PP report a patent application (10179126) issued on January 15th 2019 for the use of leriglitazone described in this paper. The patent will be owned by those authors. MM is the cofounder of Minoryx Therapeutics focused on the development of therapies for rare neurodegenerative diseases. PGC, JR and DL received a payment for their study proposals to carry out some of the studies shown in this manuscript, which just covered the purchase of the reagents and the time invested.

Acknowledgements

This work was supported by Retos-Colaboración 2017 (RTC-2017-5867-1), ENISA Jovenes Emprendedores 2012, Torres Quevedo 2017 (PTQ-17-09233) and Region Wallonne (SPW-EER/DRDT/DPjR/DEMO/ML/Déf-7939).

Appendix A. Supplementary data

Supplementary data to this article can be found online at https://doi.org/10.1016/j.nbd.2020.105162.

References

Abeti, R., Brown, A.F., Maiolino, M., Patel, S., Giunti, P., 2018. Calcium Deregulation: Novel Insights to Understand Friedreich's Ataxia Pathophysiology. Front Cell Neurosci 12, 264. https://doi.org/10.3389/fncel.2018.00264.

Anjomani Virmouni, S., Ezzatizadeh, V., Sandi, C., Sandi, M., Al-Mahdawi, S., Chutake, Y., Pook, M.A., 2015. A novel GAA-repeat-expansion-based mouse model of Friedreich's ataxia. Dis Model Mech 8, 225–235. https://doi.org/10.1242/dmm.018952.

Bencze, K.Z., Kondapalli, K.C., Cook, J.D., McMahon, S., Millán-Pacheco, C., Pastor, N., Stemmler, T.L., 2006. The structure and function of frataxin. Crit. Rev. Biochem. Mol. Biol. 41, 269–291. https://doi.org/10.1080/10409230600846058.

Bolinches-Amorós, A., Mollá, B., Pla-Martín, D., Palau, F., González-Cabo, P., 2014. Mitochondrial dysfunction induced by frataxin deficiency is associated with cellular senescence and abnormal calcium metabolism. Front Cell Neurosci 8, 124. https://doi.org/10.3389/fncel.2014.00124.

Bradley, J.L., Blake, J.C., Chamberlain, S., Thomas, P.K., Cooper, J.M., Schapira, A.H., 2000. Clinical, biochemical and molecular genetic correlations in Friedreich's ataxia. Hum. Mol. Genet. 9, 275–282.

Britti, E., Delaspre, F., Feldman, A., Osborne, M., Greif, H., Tamarit, J., Ros, J., 2018. Frataxin-deficient neurons and mice models of Friedreich ataxia are improved by TAT-MTScs-FXN treatment. J. Cell. Mol. Med. 22, 834–848. https://doi.org/10.1111/jcmm.13365.

Britti, E., Delaspre, F., Tamarit, J., Ros, J., 2020. Calpain-Inhibitors Protect Frataxin-Deficient Dorsal Root Ganglia Neurons from Loss of Mitochondrial Na+/Ca2+ Exchanger, NCLX, and Apoptosis. Neurochem. Res. https://doi.org/10.1007/s11064-020-03020-3.

Bulteau, A.L., O'Neill, H.A., Kennedy, M.C., Ikeda-Saito, M., Isaya, G., Szweda, L.I., 2004. Frataxin acts as an iron chaperone protein to modulate mitochondrial aconitase activity. Science 305, 242–245. https://doi.org/10.1126/science.1098991.

Bulteau, A.L., Planamente, S., Jornea, L., Dur, A., Lesuisse, E., Camadro, J.M., Auchère, F., 2012. Changes in mitochondrial glutathione levels and protein thiol oxidation in Δyfh1 yeast cells and the lymphoblasts of patients with Friedreich's ataxia. Biochim. Biophys. Acta 1822, 212–225. https://doi.org/10.1016/j.bbadis.2011.11.003.

Campuzano, V., Montermini, L., Lutz, Y., Cova, L., Hindelang, C., Jiralerspong, S., Trottier, Y., Kish, S.J., Faucheux, B., Trouillas, P., Authier, F.J., Dürr, A., Mandel, J. L., Vescovi, A., Pandolfo, M., Koenig, M., 1997. Frataxin is reduced in Friedreich ataxia patients and is associated with mitochondrial membranes. Hum. Mol. Genet. 6, 1771–1780.

Campuzano, V., Montermini, L., Moltò, M.D., Pianese, L., Cossée, M., Cavalcanti, F., Monros, E., Rodius, F., Duclos, F., Monticelli, A., Zara, F., Cañizares, J., Koutnikova, H., Bidichandani, S.I., Gellera, C., Brice, A., Trouillas, P., De Michele, G., Filla, A., De Frutos, R., Palau, F., Patel, P.I., Di Donato, S., Mandel, J.L., Cocozza, S., Koenig, M., Pandolfo, M., 1996. Friedreich's ataxia: autosomal recessive disease caused by an intronic GAA triplet repeat expansion. Science 271, 1423–1427.

Clay, A., Hearle, P., Schadt, K., Lynch, D.R., 2019. New developments in pharmacotherapy for Friedreich ataxia. Expert Opin Pharmacother 20, 1855–1867. https://doi.org/10.1080/14656566.2019.1639671.

Coppola, G., Marmolino, D., Lu, D., Wang, Q., Cnop, M., Rai, M., Acquaviva, F., Cocozza, S., Pandolfo, M., Geschwind, D.H., 2009. Functional genomic analysis of frataxin deficiency reveals tissue-specific alterations and identifies the PPARγ pathway as a therapeutic target in Friedreich's ataxia. Hum Mol Genet 18, 2452–2461. https://doi.org/10.1093/hmg/ddp183.

Dong, Y.N., McMillan, E., Clark, E.M., Lin, H., Lynch, D.R., 2019. GRP75 overexpression rescues frataxin deficiency and mitochondrial phenotypes in Friedreich ataxia cellular models. Hum. Mol. Genet. 28, 1594–1607. https://doi.org/10.1093/hmg/ddy448.

Fuenzalida, K., Quintanilla, R., Ramos, P., Piderit, D., Fuentealba, R.A., Martinez, G., Inestrosa, N.C., Bronfman, M., 2007. Peroxisome proliferator-activated receptor gamma up-regulates the Bcl-2 anti-apoptotic protein in neurons and induces mitochondrial stabilization and protection against oxidative stress and apoptosis. J. Biol. Chem. 282, 37006–37015. https://doi.org/10.1074/jbc.M700447200.

Gerber, J., Mühlenhoff, U., Lill, R., 2003. An interaction between frataxin and Isu1/Nfs1 that is crucial for Fe/S cluster synthesis on Isu1. EMBO Rep. 4, 906–911. https://doi.org/10.1038/sj.embor.embor918.

Gulick, T., Cresci, S., Caira, T., Moore, D.D., Kelly, D.P., 1994. The peroxisome proliferator-activated receptor regulates mitochondrial fatty acid oxidative enzyme gene expression. Proc. Natl. Acad. Sci. U.S.A. 91, 11012–11016. https://doi.org/10.1073/pnas.91.23.11012.

Gureev, A.P., Shaforostova, E.A., Popov, V.N., 2019. Regulation of Mitochondrial Biogenesis as a Way for Active Longevity: Interaction Between the Nrf2 and PGC-1α Signaling Pathways. Front Genet 10, 435. https://doi.org/10.3389/fgene.2019.00435.

Jasoliya, M.J., McMackin, M.Z., Henderson, C.K., Perlman, S.L., Cortopassi, G.A., 2017. Frataxin deficiency impairs mitochondrial biogenesis in cells, mice and humans. Hum. Mol. Genet. 26, 2627–2633. https://doi.org/10.1093/hmg/ddx141.

Jung, T.W., Lee, J.Y., Shim, W.S., Kang, E.S., Kim, S.K., Ahn, C.W., Lee, H.C., Cha, B.S., 2006. Rosiglitazone protects human neuroblastoma SH-SY5Y cells against acetaldehyde-induced cytotoxicity. Biochem. Biophys. Res. Commun. 340, 221–227. https://doi.org/10.1016/j.bbrc.2005.11.177.

Koeppen, A.H., 2011. Friedreich's ataxia: Pathology, pathogenesis, and molecular genetics. J. Neurol. Sci. 303, 1–12. https://doi.org/10.1016/j.jns.2011.01.010.

Koeppen, A.H., Michael, S.C., Knutson, M.D., Haile, D.J., Qian, J., Levi, S., Santambrogio, P., Garrick, M.D., Lamarche, J.B., 2007. The dentate nucleus in

Friedreich's ataxia: the role of iron-responsive proteins. Acta Neuropathol. 114, 163–173. https://doi.org/10.1007/s00401-007-0220-y.
Koeppen, A.H., Morral, J.A., Davis, A.N., Qian, J., Petrocine, S.V., Knutson, M.D., Gibson, W.M., Cusack, M.J., Li, D., 2009. The dorsal root ganglion in Friedreich's ataxia. Acta Neuropathol. 118, 763–776. https://doi.org/10.1007/s00401-009-0589-x.
Lee, W.-S., Kim, J., 2015. Peroxisome Proliferator-Activated Receptors and the Heart: Lessons from the Past and Future Directions. PPAR Res 2015, 271983. https://doi.org/10.1155/2015/271983.
Lin, H., Magrane, J., Rattelle, A., Stepanova, A., Galkin, A., Clark, E.M., Dong, Y.N., Halawani, S.M., Lynch, D.R., 2017. Early cerebellar deficits in mitochondrial biogenesis and respiratory chain complexes in the KIKO mouse model of Friedreich ataxia. Dis Model Mech 10, 1343–1352. https://doi.org/10.1242/dmm.030502.
Marmolino, D., Acquaviva, F., Pinelli, M., Monticelli, A., Castaldo, I., Filla, A., Cocozza, S., 2009. PPAR-gamma agonist Azelaoyl PAF increases frataxin protein and mRNA expression: new implications for the Friedreich's ataxia therapy. Cerebellum 8, 98–103. https://doi.org/10.1007/s12311-008-0087-z.
Marmolino, D., Manto, M., Acquaviva, F., Vergara, P., Ravella, A., Monticelli, A., Pandolfo, M., 2010. PGC-1alpha Down-Regulation Affects the Antioxidant Response in Friedreich's Ataxia. PLoS One 5. https://doi.org/10.1371/journal.pone.0010025.
Mincheva-Tasheva, S., Obis, E., Tamarit, J., Ros, J., 2014. Apoptotic cell death and altered calcium homeostasis caused by frataxin depletion in dorsal root ganglia neurons can be prevented by BH4 domain of Bcl-xL protein. Hum. Mol. Genet. 23, 1829–1841. https://doi.org/10.1093/hmg/ddt576.
Mollá, B., Muñoz-Lasso, D.C., Calap, P., Fernandez-Vilata, A., de la Iglesia-Vaya, M., Pallardó, F.V., Moltó, M.D., Palau, F., Gonzalez-Cabo, P., 2019. Phosphodiesterase Inhibitors Revert Axonal Dystrophy in Friedreich's Ataxia Mouse Model. Neurotherapeutics. doi:https://doi.org/10.1007/s13311-018-00706-z.
Muñoz-Lasso, D.C., Mollá, B., Calap-Quintana, P., García-Giménez, J.L., Pallardo, F.V., Palau, F., Gonzalez-Cabo, P., 2020. Cofilin dysregulation alters actin turnover in frataxin-deficient neurons. Scientific Reports 10, 5207. https://doi.org/10.1038/s41598-020-62050-7.
Navarro, J.A., Ohmann, E., Sanchez, D., Botella, J.A., Liebisch, G., Moltó, M.D., Ganfornina, M.D., Schmitz, G., Schneuwly, S., 2010. Altered lipid metabolism in a Drosophila model of Friedreich's ataxia. Hum. Mol. Genet. 19, 2828–2840. https://doi.org/10.1093/hmg/ddq183.
Obis, È., Irazusta, V., Sanchís, D., Ros, J., Tamarit, J., 2014. Frataxin deficiency in neonatal rat ventricular myocytes targets mitochondria and lipid metabolism. Free Radical Biol. Med. 73, 21–33. https://doi.org/10.1016/j.freeradbiomed.2014.04.016.
Pastore, A., Tozzi, G., Gaeta, L.M., Bertini, E., Serafini, V., Cesare, S.D., Bonetto, V., Casoni, F., Carrozzo, R., Federici, G., Piemonte, F., 2003. Actin Glutathionylation Increases in Fibroblasts of Patients with Friedreich's Ataxia: a potential role in the pathogenesis of the disease. J. Biol. Chem. 278, 42588–42595. https://doi.org/10.1074/jbc.M301872200.
Poli, S., Vilalta, A., Rodríguez-Pascau, L., Cerrada-Gimenez, M., Berger, J., Forss-Petter, S., Weinhofer, I., Musolino, P., Martinell, M., Pizcueta, P., 2020. MIN-102 (leriglitazone), a Brain Penetrant PPAR gamma Agonist, Decreases Neuroinflammation and Neurodegeneration and Promotes Re-Myelination in Preclinical Models of X-linked Adrenoleukodystrophy (X-ALD) (759). Neurology 94.
Puccio, H., Simon, D., Cossée, M., Criqui-Filipe, P., Tiziano, F., Melki, J., Hindelang, C., Matyas, R., Rustin, P., Koenig, M., 2001. Mouse models for Friedreich ataxia exhibit cardiomyopathy, sensory nerve defect and Fe-S enzyme deficiency followed by intramitochondrial iron deposits. Nat. Genet. 27, 181–186. https://doi.org/10.1038/84818.
Puigserver, P., Spiegelman, B.M., 2003. Peroxisome proliferator-activated receptor-gamma coactivator 1 alpha (PGC-1 alpha): transcriptional coactivator and metabolic regulator. Endocr. Rev. 24, 78–90. https://doi.org/10.1210/er.2002-0012.
Puigserver, P., Wu, Z., Park, C.W., Graves, R., Wright, M., Spiegelman, B.M., 1998. A cold-inducible coactivator of nuclear receptors linked to adaptive thermogenesis. Cell 92, 829–839. https://doi.org/10.1016/s0092-8674(00)81410-5.
Purroy, R., Britti, E., Delaspre, F., Tamarit, J., Ros, J., 2018. Mitochondrial pore opening and loss of Ca2+ exchanger NCLX levels occur after frataxin depletion. Biochimica et Biophysica Acta (BBA) - Molecular Basis of Disease 1864, 618–631. https://doi.org/10.1016/j.bbadis.2017.12.005.
Purroy, R., Medina-Carbonero, M., Ros, J., Tamarit, J., 2020. Frataxin-deficient cardiomyocytes present an altered thiol-redox state which targets actin and pyruvate dehydrogenase. Redox Biol 32, 101520. https://doi.org/10.1016/j.redox.2020.101520.
Qin, H., Tan, W., Zhang, Z., Bao, L., Shen, H., Wang, F., Xu, F., Wang, Z., 2015. 15d-prostaglandin J2 protects cortical neurons against oxygen-glucose deprivation/reoxygenation injury: involvement of inhibiting autophagy through upregulation of Bcl-2. Cell. Mol. Neurobiol. 35, 303–312. https://doi.org/10.1007/s10571-014-0125-y.
Shan, Y., Schoenfeld, R.A., Hayashi, G., Napoli, E., Akiyama, T., Iodi Carstens, M., Carstens, E.E., Pook, M.A., Cortopassi, G.A., 2013. Frataxin deficiency leads to defects in expression of antioxidants and Nrf2 expression in dorsal root ganglia of the Friedreich's ataxia YG8R mouse model. Antioxid. Redox Signal. 19, 1481–1493. https://doi.org/10.1089/ars.2012.4537.
Stehling, O., Elsässer, H.-P., Brückel, B., Mühlenhoff, U., Lill, R., 2004. Iron-sulfur protein maturation in human cells: evidence for a function of frataxin. Hum. Mol. Genet. 13, 3007–3015. https://doi.org/10.1093/hmg/ddh324.
Tsou, A.Y., Paulsen, E.K., Lagedrost, S.J., Perlman, S.L., Mathews, K.D., Wilmot, G.R., Ravina, B., Koeppen, A.H., Lynch, D.R., 2011. Mortality in Friedreich ataxia. J. Neurol. Sci. 307, 46–49. https://doi.org/10.1016/j.jns.2011.05.023.
Vankoningsloo, S., Piens, M., Lecocq, C., Gilson, A., De Pauw, A., Renard, P., Demazy, C., Houbion, A., Raes, M., Arnould, T., 2005. Mitochondrial dysfunction induces triglyceride accumulation in 3T3-L1 cells: role of fatty acid beta-oxidation and glucose. J. Lipid Res. 46, 1133–1149. https://doi.org/10.1194/jlr.M400464-JLR200.
Vaubel, R.A., Isaya, G., 2013. Iron-sulfur cluster synthesis, iron homeostasis and oxidative stress in Friedreich ataxia. Mol. Cell. Neurosci. 55, 50–61. https://doi.org/10.1016/j.mcn.2012.08.003.
Watmough, N.J., Bindoff, L.A., Birch-Machin, M.A., Jackson, S., Bartlett, K., Ragan, C.I., Poulton, J., Gardiner, R.M., Sherratt, H.S., Turnbull, D.M., 1990. Impaired mitochondrial beta-oxidation in a patient with an abnormality of the respiratory chain. Studies in skeletal muscle mitochondria. J. Clin. Invest. 85, 177–184. https://doi.org/10.1172/JCI114409.
Wilson, R.B., Roof, D.M., 1997. Respiratory deficiency due to loss of mitochondrial DNA in yeast lacking the frataxin homologue. Nat. Genet. 16, 352–357. https://doi.org/10.1038/ng0897-352.
Wu, J.-S., Lin, T.-N., Wu, K.K., 2009. Rosiglitazone and PPAR-gamma overexpression protect mitochondrial membrane potential and prevent apoptosis by upregulating anti-apoptotic Bcl-2 family proteins. J. Cell. Physiol. 220, 58–71. https://doi.org/10.1002/jcp.21730.